CAR-BORNE MEASUREMENTS OF ATMOSPHERIC NO_2 BY A COMPACT BROADBAND CAVITY ENHANCED ABSORPTION SPECTROMETER**

L. Ling [1,3*], Y. Huang [1,2*], A. Li [3], R. Hu [3], P. Xie [3]

[1] School of Electrical and Information Technology at Anhui University of Science and Technology, Huainan 232001, China; e-mail: lyling@aust.edu.cn
[2] Anhui Science and Technology University, Fengyang 233100, China; e-mail: hry628@163.com
[3] Key Laboratory of Environmental Optical and Technology, Anhui Institute of Optics and Fine Mechanics, Chinese Academy of Sciences, Hefei 230031, China

We report car-borne measurements of atmospheric NO_2 close to the ground by incoherent broadband cavity enhanced absorption spectroscopy (IBBCEAS). A compact IBBCEAS spectrometer with a blue light emitting diode (LED) having a central wavelength of 458 nm, a full width at half maximum of 25 nm, and a 50-cm-long cavity was developed for mobile measurements. The NO_2 detection limit of the spectrometer was calculated as 1.9 parts per billion by volume (ppbv) for a 30 s acquisition time by stabilizing the LED emitting spectrum, optimizing the NO_2 reference cross-sections, and by calibrating the reflectivity of the cavity mirrors. The accuracy of the spectrometer was verified by measuring NO_2 samples with various mixing ratios between 1–200 ppbv, which were produced by a gas dilution system in the laboratory. Three distinct journeys in Nanjing and the surrounding areas were selected as observation routes. The atmospheric NO_2 close to the ground was measured by the spectrometer from August 4 to 7, 2013. The mixing ratios of NO_2 ranged from 3 to 144 ppbv. These results were compared with the column density of NO_2 measured by a passive differential optical absorption spectroscopy (DOAS) instrument on the same car. Hence, we demonstrate the feasibility of using the spectrometer for car-borne measurements of atmospheric NO_2.

Keywords: *incoherent broadband cavity enhanced absorption spectroscopy, car-borne measurements, atmospheric NO_2.*

ИЗМЕРЕНИЯ АТМОСФЕРНОГО ДИОКСИДА АЗОТА КОМПАКТНЫМ ШИРОКОПОЛОСНЫМ СПЕКТРОМЕТРОМ УСИЛЕННОГО ПОГЛОЩЕНИЯ

L. Ling [1,3*], Y. Huang [1,2*], A. Li [3], R. Hu [3], P. Xie [3]

УДК 535.34;543.42

[1] Школа электрических и информационных технологий Аньхойского университета науки и техники, Хуайнань 232001, Китай; e-mail: lyling@aust.edu.cn
[2] Аньхойский научно-технический университет, Фэньян 233100, Китай; e-mail: hry628@163.com
[3] Аньхойский институт оптики и точной механики Китайской академии наук, Хэфэй 230031, Китай

(Поступила 17 июня 2020)

Проведены измерения атмосферного диоксида азота NO_2 вблизи земли с помощью некогерентной широкополосной спектроскопии усиленного поглощения (IBBCEA). Для мобильных измерений разработан компактный спектрометр IBBCEAS с синим светодиодом (LED) с длиной волны 458 нм, полушириной 25 нм и полостью длиной 50 см. Предел обнаружения NO_2 рассчитан как 1.9 части на миллиард по объему (ppbv) в течение 30 с сбора данных путем стабилизации спектра излучения све-

** Full text is published in JAS V. 88, No. 4 (http://springer.com/journal/10812) and in electronic version of ZhPS V. 88, No. 4 (http://www.elibrary.ru/title_about.asp?id=7318; sales@elibrary.ru).

тодиода, оптимизации эталонных сечений NO_2 и калибровки отражательной способности зеркал резонатора. Точность спектрометра проверена путем измерения образцов NO_2 с различными коэффициентами смешивания в диапазоне 1–200 ppbv, полученных с помощью системы разбавления газа в лаборатории. Наблюдения проведены во время трех отдельных маршрутов в Нанкин и прилегающие районы. Атмосферный NO_2 вблизи земли измерен спектрометром с 4 по 7 августа 2013 г. Соотношение NO_2 в смеси варьировалось от 3 до 144 ppbv. Результаты сопоставлены с плотностью NO_2, измеренной прибором пассивной дифференциальной спектроскопии оптического поглощения (DOAS) на том же автомобиле. Продемонстрирована целесообразность использования спектрометра для автомобильных измерений атмосферного NO_2.

Ключевые слова: *некогерентная широкополосная спектроскопия усиленного поглощения, мобильные измерения, атмосферный NO_2.*

Introduction. Passive differential optical absorption spectroscopy (DOAS) on a mobile platform is widely used to measure spatial and temporal distributions of atmospheric NO_2. Davis et al. [1] used mobile multi-axis differential optical absorption spectroscopy (MAX-DOAS) to estimate NO_2 and SO_2 emissions in Sarnia, Ontario; Wu et al. [2] investigated temporal and spatial distributions of SO_2 and NO_2 vertical columns in the North China Plain with mobile DOAS; Meier et al. [3] acquired maps of NO_2 column densities below aircraft using airborne imaging DOAS. All passive DOAS systems use sunlight as the light source and are thus not suitable for monitoring air at night or during rainy, snowy, cloudy, and foggy weather conditions.

Incoherent broadband cavity enhanced absorption spectroscopy (IBBCEAS), based on artificial light sources, has been developed in recent years. The IBBCEAS instrument is compact and highly sensitive and can be operated all day and night. Since IBBCEAS was first reported by Fiedler et al. [4], it has been widely applied to detect trace gases including NO_2 [5–18], CHOCHO [5, 8, 11], HONO [7, 9, 14, 15], HCHO [19], NO_3 [11, 12, 15, 20], I_2 [21], H_2O [13, 21], and aerosol [16, 22]. However, to the best of our knowledge, all these applications have been at the ground level, except for some airborne measurements of HONO, CHOCHO, NO_3, and NO_2, as reported by Kennedy et al. [9, 12, 13]. Thus, IBBCEAS has yet to be applied to other mobile platforms. The purpose of this study is to develop a compact IBBCEAS spectrometer for carborne measurements of atmospheric NO_2. NO_2 levels in Nanjing urban and surrounding areas were monitored by IBBCEAS and with a mobile DOAS system on the same car in 2013. The spectrometer's performance was assessed by analyzing the measured spectra. Mixing ratios of NO_2 retrieved from the IBBCEAS spectra were compared with the column density of NO_2 measured by the mobile DOAS system, further demonstrating the efficacy of the spectrometer.

Experimental. Figure 1a illustrates a schematic diagram of the IBBCEAS instrument, which consists of a blue LED optical source, two lenses, a filter, two mirrors with high reflectivity, a gas cell, a pump, a spectrometer, fiber cables, and a power supply. A blue LED (LZ1-00B205, LedEngin) with a peak wavelength at 458 nm and a full width at half maximum (FWHM) of 25 nm was used as the light source of the instrument. The working current was 700±1 mA, and the optical power was ~1200 mW. The LED was mounted on a temperature-controlled cooling stage to stabilize its emission spectrum. The light emitted from the LED was focused by a lens (f_1, f = 352 mm) into a 50-cm-long high-finesse cavity, which consisted of two high reflectivity dielectric mirrors (Layertec GmbH) with a high reflectivity of 0.999 over the range of 440–480 nm, a diameter of 25 mm, and a curvature radius of 1.5 m. An iris was used to reduce stray light and confine the diameter of the light spot to the first mirror M1. Out-of-band light was removed by a colored glass filter (GG420, Schott) placed behind the LED. Light transmitted through M2 was focused by an aspheric lens (f_2, f = 32 mm) into an optical fiber (with a core diameter of 400 μm and a numerical aperture of 0.22) connected to a spectrometer (QE65000, Ocean Optics) with a resolution of 0.3 nm. The sampled air was filtered using a polytetrafluoroethylene (PTFE) filter (pore size: 0.22 μm) to remove aerosols and then pumped at a flow rate of 3 slm (standard liters per min) into the cavity, which consisted of a 21-mm-internal-diameter Teflon-coated tube. The reference and absorption spectra were recorded and analyzed with a computer.

The relationship between the number density of molecules and the light intensity in the IBBCEAS has been reported by Fiedler et al. [4]:

$$\alpha(\lambda) = \sum_i \sigma_i(\lambda) N_i = \frac{1}{d}\left(\frac{I_0(\lambda)}{I(\lambda)} - 1\right)\left(1 - R(\lambda)\right), \quad (1)$$

where $\sigma_i(\lambda)$ and N_i are the absorption cross-section and the number density for species i, respectively, $I(\lambda)$ and $I_0(\lambda)$ are the transmitted intensity in the presence and absence of a sample, $R(\lambda)$ is the mirror reflectivity, and d is the physical length of the cavity. The number density of measured gases can be determined by least-squares regression of the absorption cross-section $\sigma_i(\lambda)$ and the absorption coefficient $\alpha(\lambda)$, based on Eq. (1).

The application of LED in IBBCEAS is advantageous because of its size, price, safety level, dependability, ease of handling, power consumption level, and lifetime. The radiation band of the LED matches the wavelength range of high reflectivity of the mirrors. Nevertheless, all the LEDs showed a dependence of the shape of the emission spectrum on temperature. In our previous work [23], the temperature coefficients of the central wavelength and peak intensity were +0.005 nm/°C and −0.24%/°C for a blue LED, respectively. The temperature effect was not notable, but may not be negligible in field measurements because of the potentially wide range of temperature conditions.

A closed-loop control system and a heat sink base were designed to keep the temperature of the blue LED stable (Fig. 1b). The blue LED was mounted on an aluminum heat sink whose temperature was regulated by a thermo-electric cooler (TEC). The thermal resistor PT1000 was placed as close to the LED as possible to accurately monitor the LED temperature. A microcontroller operated the proportional–integral–differential (PID) algorithm to periodically adjust the working current of the TEC on the basis of the difference between the expected and the real temperature of the LED. The final error was within ±0.1°C.

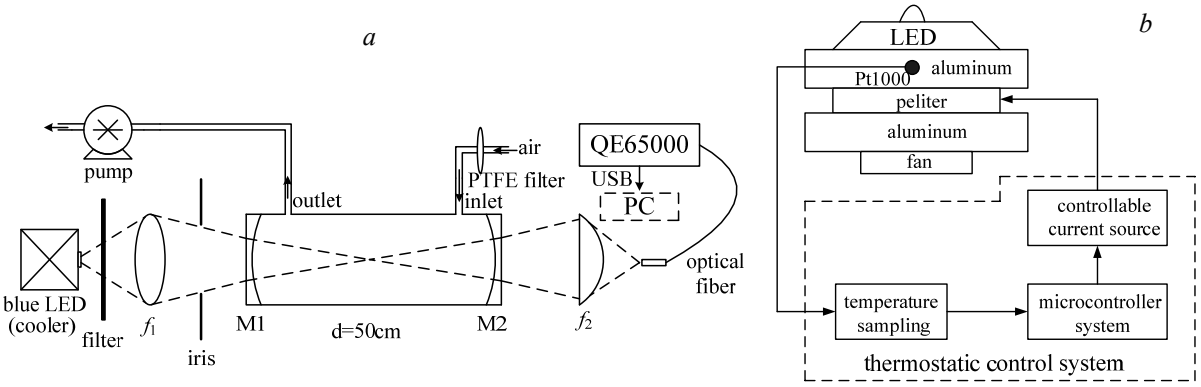

Fig. 1. Schematic diagram of the IBBCEAS instrument (a) and LED temperature control system (b).

The wavelength dependent mirror reflectivity should be determined for quantitative absorption measurements in accordance with Eq. (1). In the present instrument, the mirror reflectivity was determined by the difference in the transmitted light intensity when the cavity was separately filled with N_2 and He, as described by Washenfelder et al. [24]

$$R(\lambda) = 1 - d\,\frac{\dfrac{I_{N_2}(\lambda)}{I_{He}(\lambda)}\alpha_{Ray}^{N_2}(\lambda) - \alpha_{Ray}^{He}(\lambda)}{1 - I_{N_2}(\lambda)/I_{He}(\lambda)}, \qquad (2)$$

where $I_{N2}(\lambda)$ and $I_{He}(\lambda)$ are the intensities of N_2 and He absorption spectra, and $\alpha_{Ray}^{He}(\lambda)$ and $\alpha_{Ray}^{N_2}(\lambda)$ represent the optical extinction governed by Rayleigh scattering of He and N_2, respectively. In our measurements, $I_{N2}(\lambda)$ and $I_{He}(\lambda)$were both recorded at ambient temperature (297 K) and pressure (1013 mbar) when the cavity was flushed with pure N_2 (purity of 0.99999) and pure He (purity of 0.99999), respectively. The extinction owing to Rayleigh scattering was equal to the product of the Rayleigh scattering cross-section and the number density corresponding to the purity of the gases. The Rayleigh scattering cross-sections of N_2 and He were interpolated to obtain the cross-sectional values over the region of interest based on the cross-sectional value of N_2 at 457.9 nm measured by Shardanand et al. [25] and He at 532 nm measured by Sneep et al. [26] and the dependence on wavelength (proportional to $\lambda^{-4.082}$).

Figure 2b shows the extinctions owing to Rayleigh scattering of pure He and N_2 in the present case. The calibrated mirror reflectivity (not filtered) in the region of 435–485 nm is shown in Fig. 2a. The roughness of the mirror reflectivity at both ends of the wavelength range is attributed to the defects of the optical filter or the detector. The maximum reflectivity of ~0.9987 was found at 458 nm, corresponding to an effective path length of ~384 m.

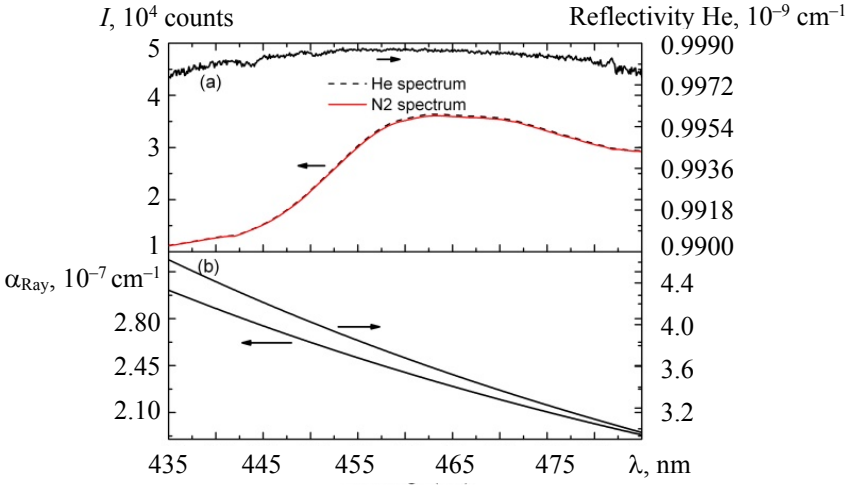

Fig. 2. (a) Absorption spectra of pure He (black dash) and pure N_2 (red). Solid black line is the calibrated mirror reflectivity; (b) extinction owing to Rayleigh scattering of pure He and N_2.

The concentrations (or mixing ratios) of the target gases were determined by least-squares regression of their reference cross-sections and the absorption coefficient. In applications of broadband absorption spectroscopy, to obtain the reference cross-section it is common to convolute the high-resolution cross-section reported in the literature with the slit function of the spectrometer. However, this method only considers the characteristics of the spectrometer rather than the measurement system. In the present work, the reference cross-section of NO_2 was obtained in two steps: (1) The profile of the NO_2 cross-section, $\sigma^P_{NO_2}(\lambda)$, was obtained by filling the cavity with a NO_2 sample diluted in pure N_2 and recording its absorption spectrum, $I_{NO_2}(\lambda)$:

$$\sigma^P_{NO_2}(\lambda) = \frac{1}{N_{NO_2}} \frac{1}{d} \left(\frac{I_{N_2}(\lambda)}{I_{NO_2}(\lambda)} - 1 \right) \left(1 - R(\lambda)\right), \tag{3}$$

where N_{NO2} is the number density of the NO_2 sample, which can be assigned any value. (2) The profile of the NO_2 cross-section was then scaled to the reference cross-section of NO_2 with the known value of the high-resolution section at a certain wavelength (absorption peak of 448 nm in our work) in the literature [27].

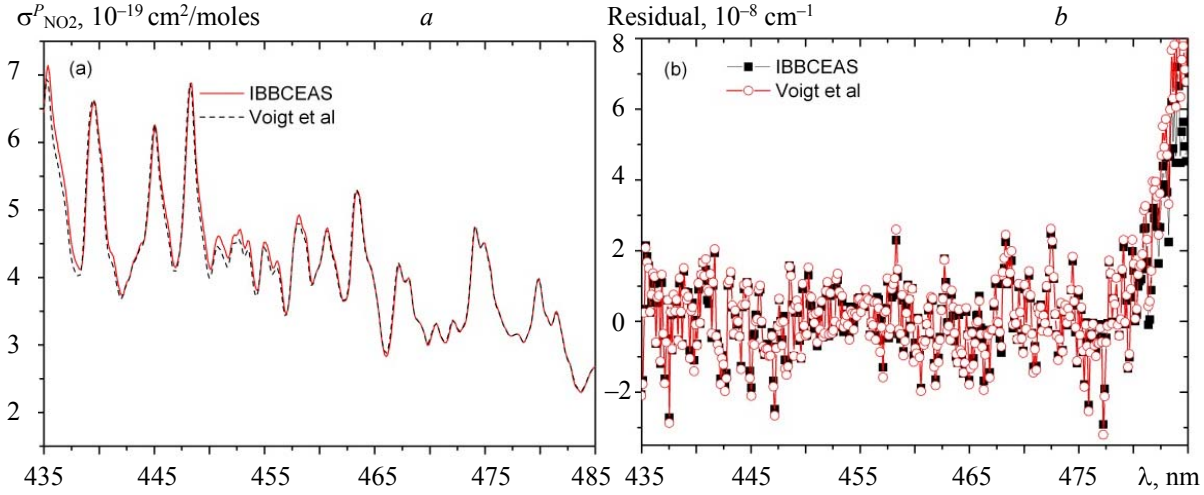

Fig. 3. (a) Reference cross-section of NO_2 obtained by the common method (red) and the method proposed in this study (black dashed line); (b) residuals of fitting the reference cross section of NO_2 obtained by the common method (red) and the proposed method in this paper (black dash) to the same NO_2 absorption spectrum. The 1 σ noise (standard deviation of the fitting residual) values were 1.63×10^{-8} cm^{-1} (red) and 1.57×10^{-8} cm^{-1} (black).

Figure 3 compares the reference cross-section of NO_2 obtained from the NO_2 sample absorption (i.e., IBBCEAS marked in Fig. 3a) and that obtained by convolution of the high-resolution cross-section (from Voigt et al. [27]) with the slit function of the spectrometer (i.e., Voigt et al. marked in Fig. 3a). The NO_2 reference cross-sections obtained by the two methods showed minor differences. Taking the same measured NO_2 absorption spectrum as an example, we determined the NO_2 concentrations from the NO_2 reference cross-sections obtained by both methods. Figure 3b shows the fitting residuals, which indicate that the residual of IBBCEAS was slightly lower than that of Voigt et al. The lower the fitting residual, the more accurate the reference cross-section of NO_2.

The spectrometer measurements were validated with the use of dilute standard NO_2 samples at 1 atm total pressure and with mixing ratios from 200 to 1 part per billion by volume (ppbv), which were generated by dilution of a 250-ppbv NO_2 standard mixture with pure N_2. Figure 4 shows the dilution system used to validate the spectrometer. A mass flow controller (MFC 1) was placed at the outlet of a pure N_2 cylinder to control the flow rate. Another MFC (MFC 2) was located at the outlet of the cavity to control the total flow rate of the mixture gas through the cavity. The 250 ppbv NO_2 standard gas was mixed with, and diluted by, pure N_2 before entering the cavity. The NO_2 mixing ratio after dilution was determined from the difference between the flow rate at the exit of the cavity (set by MFC 1) and the flow rate of pure N_2 (set by MFC 2). Therefore, various NO_2 samples with known mixing ratios of less than 250 ppbv were obtained by changing the flow rates. Note that MFC 2 was placed at the outlet of the cavity, rather than the NO_2 cylinder, to accurately obtain the dilute standard NO_2 samples. When dilute NO_2 mixtures pass through an MFC, considerable wall losses occur, depending on the flow rate, which makes it difficult to reliably estimate the concentration. Our scheme avoids dilute NO_2 passing through an MFC until after it has been optically probed.

The mixing ratios of the NO_2 samples measured by the spectrometer are shown in Fig. 5 and compared with the mixing ratios calculated from the flow rates. The linear regression line had a slope of 1.025±0.004 and an intercept of −0.386±0.351 ppbv, with a linear correlation factor of 0.99995. These outcomes suggest that the spectrometer was able to quantitatively determine the NO_2 mixing ratios.

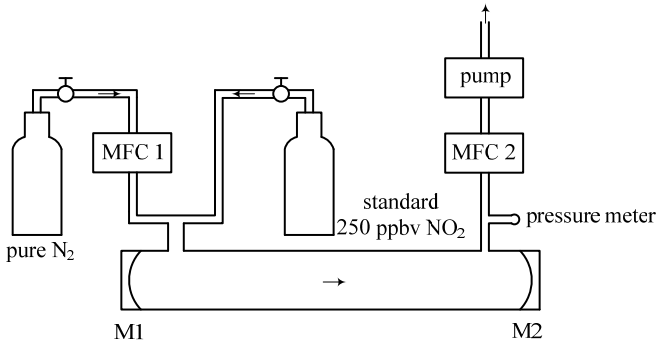

Fig. 4. Schematic diagram of the dilution system for generating NO_2 samples with mixing ratios ranging from 200 to 1 ppbv.

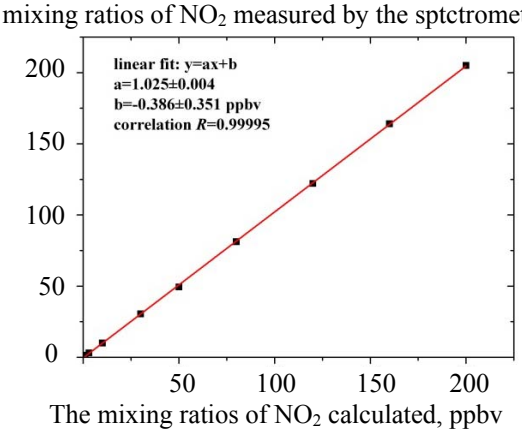

Fig. 5. Comparison and correlation of NO_2 mixing ratios measured by the spectrometer and calculated from the flow rates.

Results and discussion. Three journeys in Nanjing and surrounding areas were used as observation routes, during which the atmospheric NO_2 close to the ground was measured by the spectrometer from August 4 to 7 in 2013. The spectrometer was placed in a car along with a passive DOAS instrument. The solar tracker component of the passive DOAS instrument was placed outside of the automobile sunroof together with the sample inlet of the spectrometer. This left an unsealed space in the automobile. On hot August days, this defect in the vehicle sealing led to temperatures as high as 40°C inside the automobile, even when the air conditioner was turned on. These conditions reduced the peak intensities by 5%, although the main wavelength of the blue LED spectrum increase by 0.1 nm compared with room temperature of 20°C. Therefore, it was necessary to maintain the temperature of the blue LED used in the IBBCEAS spectrometer. In the field study, the blue LED temperature was maintained at 20±0.1°C with the homemade temperature control system described above. Furthermore, the charge-coupled-device (CCD) detector of the spectrometer was cooled to −15°C to reduce measurement noise induced by temperature fluctuations. The spectrometer was fixed on a damping plate to increase mechanical stability when the car ran. In addition, a global positioning system (GPS) and a simple meteorological station were placed in the car to record the travel route, temperature, humidity, and the wind velocity and direction.

In the optimal wavelength region of 437–479 nm used for measurements of atmospheric NO_2, absorption by ozone, water vapor, and O_2–O_2 collisional pairs, as well as optical power losses resulting from scattering by aerosols, were observed. Absorption from aerosols was negligible owing to the PTFE filter connecting the inlet tube, which was used to prevent aerosols from entering the cavity and contaminating the cavity mirrors. The performance of the PTFE filter was predicted from the changes in the intensity of the recorded spectra. The change in light intensity caused by absorption of trace gases in the atmosphere (except for a heavily polluted environment) is usually negligible, especially when the mirror reflectivity is moderate. An atmospheric spectrum recorded with the PTFE filter was compared with another recorded without the filter. A large decrease (~10%) in the intensity was observed when the filter was removed, whereas the light intensity was almost the same as that of the N_2 reference spectrum when the filter was used. This difference suggests that aerosols were effectively prevented from entering the cavity. The maximal absorption cross-section was 4.5×10^{-22} cm^2/molecule at 462 nm, which yielded a peak absorption of 3.4×10^{-10} cm^{-1} for 30 ppbv ozone in the atmosphere. The maximal absorption was approximately 1.5×10^{-9} cm^{-1} at 472 nm for a water vapor mixing ratio of 0.6% (48% relative humidity at 284 K). During the field study, the local relative humidity was always less than 50% as measured with a hygrometer in the automobile, which indicated that the maximal absorption of water vapor was slightly higher than 1.5×10^{-9} cm^{-1}. Owing to the squared dependence of the O_2–O_2 concentration on oxygen (~21% for O_2 in the atmosphere), absorption of O_2–O_2 in the air is approximately 1.78×10^{-8} cm^{-1} at the peak wavelength of 477 nm. Generally, the standard deviation of the fitting residual spectrum accounted for the detection sensitivity of the IBBCEAS instrument. The detection sensitivity of our instrument was at the level of 10^{-8} cm^{-1}. Therefore, the most frequently detected absorber other than the target molecule of NO_2 was O_2–O_2 based on absorption measurements in the optimal region of 437–479 nm.

Figure 6 shows an example of atmospheric NO_2 results measured by the IBBCEAS spectrum. The data were recorded at 10:00 on 4 August with an acquisition time of 30 s. The reference cross-section of NO_2 was obtained by the method proposed above whereas that of O_2–O_2 was determined by convoluting the high-resolution cross-section measured by Greenblatt et al. [28] with the instrument function of the spectrometer. The mixing ratio of NO_2 was 29.37 ppbv with a fitting uncertainty of 0.54 ppbv, and the 1 σ noise (standard deviation) of the residual was 1.78×10^{-8} cm^{-1}, which indicates that the detection limit for the IBBCEAS instrument was ≈1.9 ppbv.

Mobile measurements of atmospheric NO_2 with the developed spectrometer were performed around Nanjing City and its surrounding areas for 3 days. From 9:50 to 11:46 on 4 August, the automobile moved the spectrometer around Nanjing City. During that time, the mixing ratios of NO_2 ranged from 9 to 72 ppbv. The automobile entered the Laoshan tunnel at 10:39 and exited the tunnel at 10:42. During these 4 min, there was an increase in the NO_2 mixing ratio compared with the ratio measured before entering or after exiting the tunnel, owing to vehicle exhaust gas accumulation in the tunnel. The automobile started from Nanjing at 13:17 on 4 August to go east to Nantong and arrived in Chenqiao at 16:26. The next morning at 9:20, the automobile continued to go south to Suzhou and Huzhou, and then travelled west and back to Nanjing at 15:16 on 5 August. This route formed a large circle encompassing Tai Lake, a chemical plant, a cement factory, and two power plants. In mobile measurements, the mixing ratios of NO_2 ranged from 7 to 144 ppbv. High concentrations of NO_2 were not observed around the power plants or the chemical plant; however, in high-

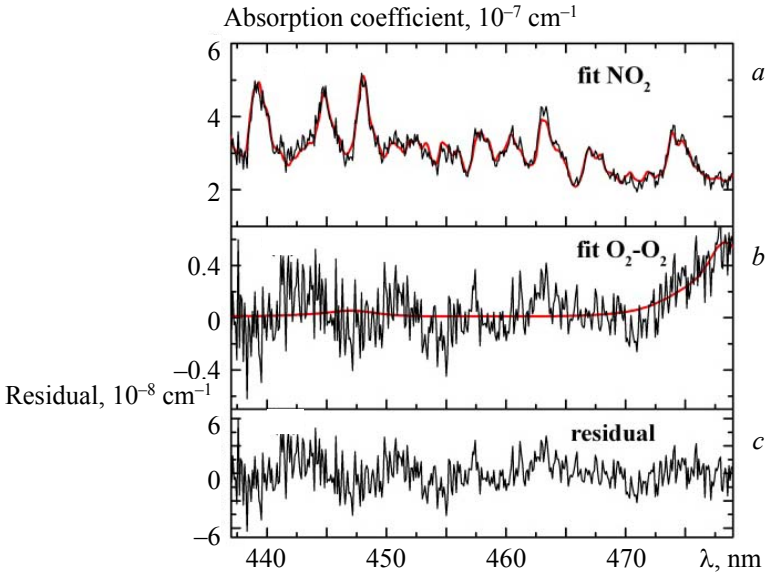

Fig. 6. Example of retrieved and fitted absorption of atmospheric NO_2 in the optimal spectral region of 437–479 nm. Spectra were recorded with 30 s exposure time (integration time 1.5 s, spectra average of 20). (a) Measured (black) and fitted (red) NO_2 spectrum. Mixing ratio of NO_2 was 29.37 ppbv. (b) Measured (black) and fitted (red) O_2–O_2 spectrum. (c) Fitting residual for which the 1 σ noise (standard deviation) was 1.78×10^{-8} cm^{-1}.

way service areas where many drivers stopped for a short rest, high NO_2 emissions were measured near the ground. Most NO_2 emissions from the chemical plant or the power plants are released into the upper atmosphere via chimneys; however, the spectrometer only measured NO_2 in the area ~2 m above the ground. In addition, despite the high concentration of particulate matter near the cement factory, light intensity did not markedly decrease, indicating the excellent performance of the PTFE filter. The feasibility of using the developed spectrometer was also demonstrated by performing measurements at a background station, which was located in an ecological scenic area in Gucheng Lake, Gaochun county. There were no point sources in the area, and only a small amount of pollution emitted from motor vehicles and human activities. The background station was 100 km south of Nanjing city. The automobile started from Nanjing at 8:50 on 7 August and arrived at the station at 10:26. The mixing ratios of NO_2 ranging from 3 to 53 ppbv. High mixing ratios were mainly observed in the urban area, and lower mixing ratios were observed farther away from the city.

No mobile measurements were performed at night because the passive DOAS instrument requires sunlight as the light source; therefore, we were unable to simultaneously measure NO_2 in the atmosphere with both instruments at night. Moreover, the field study did not aim to monitor low emissions at night because there are fewer vehicles on the road and polluting enterprises stop production at night.

To further demonstrate the performance of the developed spectrometer, we compared the atmospheric NO_2 measurements of the spectrometer with those of the passive DOAS instrument in the same automobile. Passive DOAS technology uses the sunlight at its zenith as a light source to calculate the vertical column density and spatial distribution of trace gases in the atmosphere by measuring the ultraviolet/visible absorption spectrum of the zenith sunlight. The passive DOAS instrument was able to measure atmospheric NO_2 and SO_2 in the atmosphere. It is impractical to directly compare the measurements of these two instruments because they produce results with different units. Nevertheless, the NO_2 concentrations measured by the two instruments were consistent, verifying the performance of the developed spectrometer.

Taking the latitude as the *x*-axis, longitude as the *y*-axis, and NO_2 concentrations as the *z*-axis, we plotted three-dimensional graphs of the mobile measurements of the two instruments (Fig. 7). For the passive DOAS instrument, some data are missing because of the blocked sunlight in the tunnel. In Figures 7a,b, the NO_2 column density measured by the passive DOAS instrument was very low and uniform, whereas the mixing ratios of NO_2 measured by the developed spectrometer varied considerably, which indicated that NO_2 emissions were mainly from vehicle exhaust and captured by the spectrometer. Figures 7d,e show that NO_2 concentrations near the ground mainly came from vehicle exhaust emissions and were captured by the

our spectrometer. At the same time, the passive DOAS instrument also captured some NO_2 with a high column density, which was mainly in areas around the chemical plant and power plants. The results from the two instruments were in good agreement (maximum correlation coefficient in Fig. 7i) at the background station (Fig. 7g,h), owing to the uniform air mixing, low vehicle exhaust emissions, and no high-altitude emissions from the chemical plant or the power plants. These findings demonstrate the reliability of the IBBCEAS.

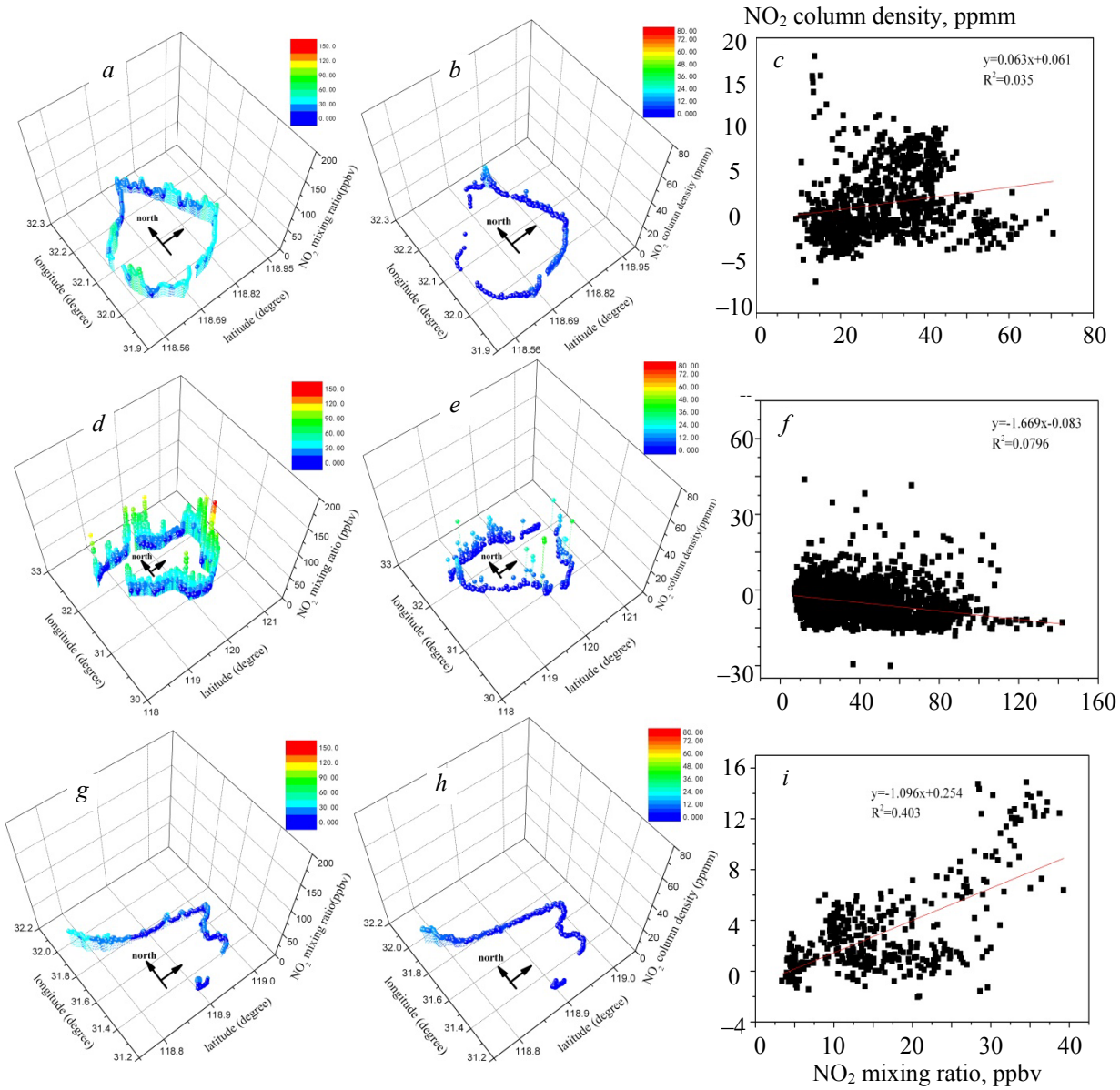

Fig. 7. Three-dimensional figures of the mobile measurements of the spectrometer (a, d, g) and the passive DOAS instrument (b, e, h) for atmospheric NO_2 around Nanjing City, following a large circle route encompassing Tai Lake, a chemical plant, a cement factory, and two power plants, and from Nanjing urban center to an atmospheric observation background station, respectively. Correlation plot (c, f, i) for NO_2 measured by the spectrometer and the passive DOAS instrument.

For long-term car-borne measurements, vibration and temperature fluctuation may degrade the performance of the IBBCEAS spectrometer. Vibrations could cause optical path deviation, resulting in a considerable decrease in the intensity of the IBBCEAS spectrum. Temperature fluctuations mainly affect the stability of the LED spectrum. In our present work, the blue LED temperature was controlled and set to be 20°C with

the use of the homemade temperature control system described above. From the real-time recorded LED temperature data, we found that the maximum fluctuation amplitude of the blue LED temperature was approximately 2°C, which caused some drift of the center wavelength of LED spectrum of approximately 0.01 nm and the light intensity of approximately 0.5%. These drifts had almost no effects on the car-borne measurements. To evaluate the influence of vibrations and temperature fluctuations on the spectrometer, we recorded the nitrogen absorption spectra at 30 min intervals and then compared the peak intensity and wavelengths of all the recorded spectra. The peak wavelength was unchanged, whereas the peak intensity had a maximum fluctuation of less than 0.6%. The influence of vibrations and temperature on the measured spectrum was very small, which confirms the high stability of the spectrometer.

Conclusions. A compact incoherent broadband cavity enhanced absorption spectrometer based on a blue LED as the light source was developed and applied during a car journey in three stages between 4 and 7 August 2013. The quantitative performance of the spectrometer was validated with standard samples of NO_2 prepared with the mixing ratios of 200–1 ppbv and was further improved by keeping the LED temperature stable and optimizing the reference cross-section of NO_2. Long-time mobile measurements of atmospheric NO_2 showed that the spectrometer was sensitive and accurate for measuring NO_2. Mixing ratios of NO_2 retrieved from the IBBCEAS spectra were compared with the column density of NO_2 measured by another passive DOAS system on the same car, confirming the usefulness of the spectrometer for car-borne measurements.

This work was supported in part by Anhui Province Key R&D Program of China under Grant 202004i07020011, and in part by the National Natural Science Foundation of China under Grant 41305139, 41530644, 41775029, and 91644107. We thank Andrew Jackson, PhD, from Liwen Bianji, Edanz Group China (www.liwenbianji.cn/ac), for editing the English text of a draft of this manuscript.

REFERENCES

1. Z. Y. W. Davis, S. Baray, C. A. McLinden, A. Khanbabakhani, W. Fujs, C. Csukat, J. Debosz, R. McLaren, *Atm. Chem. Phys.*, **19**, 13871–13889 (2019).
2. F. C. Wu, P. H. Xie, A. Li, F. S. Mou, H. Chen, Y. Zhu, T. Zhu, J. G. Liu, W. Q. Liu, *Atm. Chem. Phys.*, **18**, 1535–1554 (2018).
3. A. C. Meier, A. Schonhardt, T. Bosch, A. Richter, A. Seyler, T. Ruhtz, D. E. Constantin, R. Shaiganfar, T. Wagner, A. Merlaud, M. Van Roozendael, L. Belegante, D. Nicolae, L. Georgescu, J. P. Burrows, *Atm. Meas. Tech.*, **10**, 1831–1857 (2017).
4. S. E. Fiedler, A. Hese, A. A. Ruth, *Chem. Phys. Lett.*, **371**, 284–294 (2003).
5. S. X. Liang, M. Qin, P. H. Xie, J. Duan, W. Fang, Y. B. He, J. Xu, J. W. Liu, X. Li, K. Tang, F. H. Meng, K. D. Ye, J. G. Liu, W. Q. Liu, *Atm. Meas. Tech.*, **12**, 2499–2512 (2019).
6. N. Jordan, C. Z. Ye, S. Ghosh, R. A. Washenfelder, S. S. Brown, H. D. Osthoff, *Atm. Meas. Tech.*, **12**, 1277–1293 (2019).
7. J. Duan, M. Qin, B. Ouyang, W. Fang, X. Li, K. D. Lu, K. Tang, S. X. Liang, F. H. Meng, Z. K. Hu, P. H. Xie, W. Q. Liu, R. Haesler, *Atm. Meas. Tech.*, **11**, 4531–4543 (2018).
8. B. Fang, W. X. Zhao, X. Z. Xu, J. C. Zhou, X. Ma, S. Wang, W. J. Zhang, D. S. Venables, W. D. Chen, *Opt. Express*, **25**, 26910–26922 (2017).
9. K. E. Min, R. A. Washenfelder, W. P. Dube, A. O. Langford, P. M. Edwards, K. J. Zarzana, J. Stutz, K. Lu, F. Rohrer, Y. Zhang, S. S. Brown, *Atm. Meas. Tech.*, **9**, 423–440 (2016).
10. L. Y. Ling, P. H. Xie, M. Qin, W. Fang, Y. Jiang, R. Z. Hu, N. N. Zheng, *Chin. Opt. Lett.*, **11**, 063001 (2013).
11. T. Wu, C. Coeur-Tourneur, G. Dhont, A. Cassez, E. Fertein, X. D. He, W. D. Chen, *J. Quant. Spectrosc. Radiat. Transf.*, **133**, 199–205 (2014).
12. O. J. Kennedy, B. Ouyang, J. M. Langridge, M. J. S. Daniels, S. Bauguitte, R. Freshwater, M. W. McLeod, C. Ironmonger, J. Sendall, O. Norris, R. Nightingale, S. M. Ball, R. L. Jones, *Atm. Meas. Tech.*, **4**, 1759–1776 (2011).
13. S. X. Liang, M. Qin, J. Duan, W. Fang, A. Li, J. Xu, X. Lu, K. Tang, P. H. Xie, J. G. Liu, W. Q. Liu, *Acta Phys. Sin.*, **66**, 090704 (2017).
14. Y. Nakashima, Y. Sadanaga, *Anal. Sci.*, **33**, 519–524 (2017).
15. H. M. Yi, T. Wu, G. S. Wang, W. X. Zhao, E. Fertein, C. Coeur, X. M. Gao, W. J. Zhang, W. D. Chen, *Opt. Express*, **24**, A781 (2016).

16. M. L. Dong, W. X. Zhao, Y. Cheng, C. J. Hu, X. J. Gu, W. J. Zhang, *Acta Phys. Sin.*, **61**, 060702 (2012).
17. L. Y. Ling, P. H. Xie, P. P. Lin, Y. R. Huang, M. Qin, J. Duan, R. Z. Hu, F. C. Wu, *Acta Phys. Sin.*, **64**, 130705 (2015).
18. T. Wu, W. Zhao, W. Chen, W. Zhang, X. Gao, *Appl. Phys. B*, **94**, 85–94 (2009).
19. J. W. Liu, X. Li, Y. M. Yang, H. C. Wang, C. L. Kuang, Y. Zhu, M. D. Chen, J. L. Hu, L. M. Zeng, Y. H. Zhang, *Anal. Chem.*, **92**, 2697–2705 (2020).
20. W. P. Kong, T. Wu, W. Nie, Z. Xu, R. Lai, X. D. He, W. D. Chen, Z. P. Chen, *Acta Opt. Sin.*, **39**, 023001 (2019).
21. C. Bahrini, A. C. Gregoire, D. Obada, C. Mun, C. Fittschen, *Opt. Laser Technol.*, **108**, 466–479 (2018).
22. L. S. Meng, G. X. Wang, P. Augustin, M. Fourmantin, Q. Gou, E. Fertein, T. N. Ba, C. Coeur, A. Tomas, W. D. Chen, *Opt. Lett.*, **45**, 1611–1614 (2020).
23. L. Y. Ling, P. H. Xie, M. Qin, N. N. Zheng, C. L. Ye, A. Li, R. Z. Hu, *Spectrosc. Spectr. Anal.*, **32**, 2886–2890 (2012).
24. R. A. Washenfelder, A. O. Langford, H. Fuchs, S. S. Brown, *Atm. Chem. Phys.*, **8**, 7779–7793 (2008).
25. S. Shardanand, A. D. P. Rao, *NASA Technical Note* (1977).
26. M. Sneep, W. Ubachs, *J. Quant. Spectrosc. Radiat. Transf.*, **92**, 293–310 (2005).
27. S. Voigt, J. Orphal, J. P. Burrows, *J. Photochem. Photobiol. A*, **149**, 1–7 (2002).
28. G. D. Greenblatt, J. J. Orlando, J. B. Burkholder, A. R. Ravishankara, *J. Geophys. Res.*, **95**, 18577–18582 (1990).